Transport of inertial particles by viscous streaming in arrays of oscillating probes

Kwitae Chong, Scott D. Kelly, Stuart T. Smith, and Jeff D. Eldredge

Phys. Rev. E **93**, 013109 — Published 7 January 2016

DOI: 10.1103/PhysRevE.93.013109

Transport of inertial particles by viscous streaming in arrays of oscillating probes

Kwitae Chong,[1] Scott D. Kelly,[2] Stuart T. Smith,[2] and Jeff D. Eldredge[1,*]

[1] *Mechanical and Aerospace Engineering, University of California, Los Angeles, Los Angeles, CA 90095, United States*

[2] *Mechanical Engineering and Engineering Science, The University of North Carolina at Charlotte, Charlotte, NC 28223, United States*

(Dated: December 4, 2015)

A mechanism for the transport of micro-scale particles in viscous fluids is demonstrated. The mechanism exploits the trapping of such particles by rotational streaming cells established in the vicinity of an oscillating cylinder, recently analyzed in previous work. The present work explores a strategy of transporting particles between the trapping points established by multiple cylinders undergoing oscillations in sequential intervals. It is demonstrated that, by controlling the sequence of oscillation intervals, an inertial particle is effectively and predictably transported between the stable trapping points. Arrays of cylinders in various arrangements are investigated, revealing a technique for constructing arbitrary particle trajectories. It is found that the domain from which particles can be transported and trapped by an oscillator is extended, even to regions in which particles are shielded, by the presence of other stationary cylinders. The timescales for transport are examined, as are the mechanisms by which particles are drawn away from an obstacle toward the trapping point of an oscillator.

* Author to whom correspondence should be addressed. Electronic mail: eldredge@seas.ucla.edu

I. INTRODUCTION

Technological advances in cellular engineering, medical diagnostics and microfluidics have motivated the need to separate, collect and transport micrometer-size particles. In recent years, a variety of mechanisms have been exploited for such purposes, including dielectrophoresis [1, 2], optofluidics [3–5], inertial hydrodynamics [6–8], among others. Another mechanism, viscous streaming, has recently been demonstrated as a viable candidate for particle manipulation [9–17].

Viscous streaming is a steady secondary flow that develops from the coherent non-linear interactions within an oscillatory flow. The Reynolds stress generated by these non-linear interactions of the primary oscillatory flow inside a thin oscillatory Stokes layer drive a secondary steady streaming flow. For example, a cylinder vibrating rectilinearly normal to its axis will generate steady rotational cells in its vicinity, as shown by the gray circulatory cell rotating clockwise in figure 1(a). Reynolds stress decays exponentially from the cylinder and thus the fluid outside the inner cell is set into steady flow rotating counter clockwise, indirectly dragged by the inner streaming cell flow. These inner and outer streaming cells collectively compose the steady streaming flow. The thickness of the Stokes layer is $\delta_{AC} = (\nu/\Omega)^{1/2}$, where ν is kinematic viscosity and Ω is the angular frequency of oscillation, and this thickness is significantly smaller than reference length, cylinder radius R, when the Reynolds number, $Re = \Omega R^2/\nu$, is $O(10)$ and higher.

The mechanisms that give rise to viscous streaming flows, as well as their parametric dependencies, have been revealed by a rich body of work, both experimental and theoretical, conducted over the last several decades. Most theoretical studies have relied on an asymptotic analysis, based in some fashion on small oscillation amplitude. Schlichting [18] matched the inner layer solution, in which appropriate length scale is Stokes layer thickness δ_{AC}, with an outer solution based on unsteady Stokes flow. Riley [19] and Stuart [20] revealed the existence of an outer boundary layer in the case of large streaming Reynolds number, $Re_s = \Omega A^2/\nu \gg 1$, where A is the oscillation amplitude. The steady streaming velocity in this outer flow decays to zero. Holtsmark *et al.* [21] also performed asymptotic expansion with small oscillation amplitude ratio $\epsilon = A/R \ll 1$. In their work, they did not treat the inner and outer boundary layer separately, but rather, calculated the entire flow at each asymptotic level. The results of Holtsmark *et al.* [21] contain the solution of Schlichting [18] for $Re \gg 1$. Raney *et al.* [22] corrected the difference between theory and experiment from Holtsmark et al. by accounted for Stokes drift, which is the difference between Lagrangian streamlines (i.e. mean fluid particle trajectories) and streamlines of the mean flow.

Previous studies have demonstrated experimentally that the cells generated in a streaming flow can trap and transport inertial particles within a domain of influence inside this flow. Lutz et al. [13] visualized the three-dimensional streaming eddies generated by fluid oscillation around a fixed cylinder in a microchannel and demonstrated inertial particle trapping inside such eddies [12]. Recently, House et al. [14] exhibited particle trapping in arrays of fixed cylinders experimentally and computationally. The mechanism is also effective in the streaming cells generated by oscillating bubbles. Marmottant and Hilgenfeldt [9, 10] demonstrated vesicle transport via oscillating bubbles mounted on the substrate of a microchannel by breaking the symmetry by placing additional bumps in the vicinity of the bubble. Later, Wang *et al.* [11] selectively trapped and released micron-sized inertial particles based on the size of particle with oscillating bubbles in a Poiseuille flow. Xu and co-workers [15, 16] demonstrated that *C. elegans* can be manipulated to travel along a square loop of oscillating bubbles by turning on and off the actuator when the worm is in-line with the path.

In recent work [17], we investigated the mechanisms by which this particle trapping occurs, using an analytical model for particle transport in the flow field generated by a cylinder oscillating rectilinearly in a quiescent fluid (see figure 1(a)). An inertial particle in such a flow follows a spiraling trajectory, as shown in the figure, and becomes trapped inside the center of the streaming cell. It was shown in [17] that an inertial particle will be trapped regardless of its relative size, density and Reynolds number, provided that the particle is smaller than the characteristic size of the oscillator. The Saffman lift force [23]—an inertial force that acts upon a particle moving within a shear flow—is primarily responsible for this trapping mechanism, and Stokes drag is the dominant resistance of this trapping. As particle size decreases, the time required to trap the inertial particle increases. The final trapping location is insensitive to particle size and density.

As previous works have shown, this trapping mechanism can form the basis for a transport strategy. However, the experimental demonstrations of transport have generally relied on a single forcing that simultaneously affects all oscillators, either via the flow past fixed obstacles or an array of bubbles mounted on a substrate. In such scenarios, transport has been effected through a steady background component of the flow [11], through symmetry-breaking obstacles [9, 10], or through modulation of the forcing signal [15, 16]. However, another logical transport approach is to independently force each oscillator in an array. For example, one could conceive a strategy wherein cylinders in an array each vibrate for a finite interval, in sequence, thereby creating and annihilating streaming cells, and moving particles from one trapping point to another. Such a scenario is depicted in figure 1(b). That such a transport strategy has not been previously explored is most likely due to the inherent challenges of physically constructing an array in

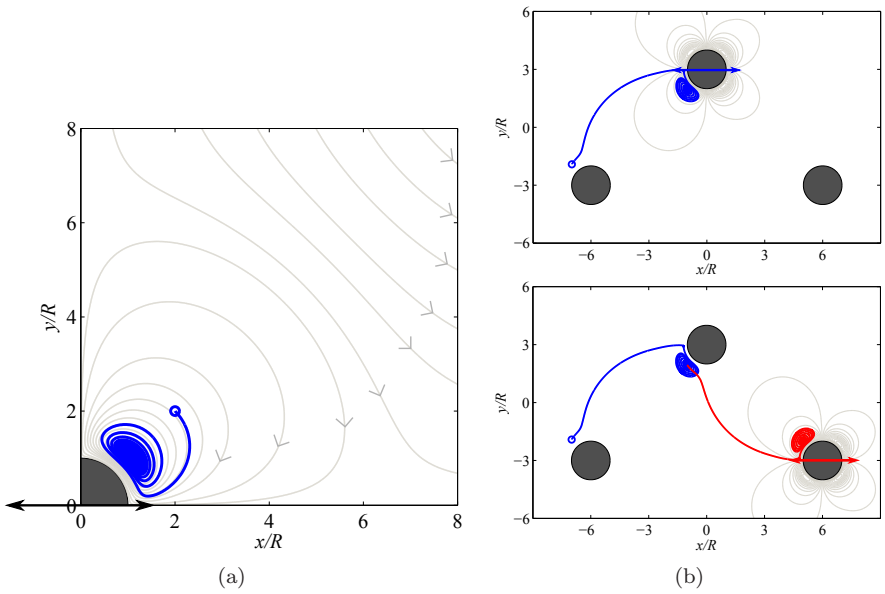

FIG. 1. (a) Inertial particle trajectory (darker line, blue online) inside streaming cell based on time-averaged Lagrangian streamline (gray line) for $Re = 40$. Initial location is depicted with a circle. Reprinted with permission from Chong *et al.*, Phys. Fluids 25, 033602 (2013). Copyright 2013, American Institute of Physics. (b) Schematic of transport of inertial particle in arrays of cylinders. Inertial particle is transported from the lower left cylinder to the upper cylinder (top), and from the upper cylinder to the lower right cylinder (bottom) by sequential oscillation of cylinders.

which each oscillator can be selectively controlled.

In this work, we explore the capabilities of an array of independently-controlled oscillators to transport inertial particles in a fluid. In order to enable such a demonstration, we rely here on high-fidelity numerical simulations of the streaming flow, and predict particle trajectories within this flow with the transport model utilized in our previous work [17]. Such a computational investigation of this problem carries its own set of challenges. As discussed below, streaming flows have a diverse set of time scales, each of which must be resolved in order to compute both the time-varying force on the particle and its net transport over many (thousands of) cycles of oscillations. Furthermore, the streaming flow itself—an essential component of the transport effector—is only a weak product of the most energetic components of the fluid motion and therefore difficult to capture numerically, particularly in the intermediate regions between oscillators, where it is weakest. Though we use some techniques to recover some computational efficiency, as described below, each transport case requires significant time and effort to study in a manner in which physical fidelity is fully preserved.

For these reasons, this work focuses on exploring particle transport in a somewhat limited parametric regime; a single Reynolds number and particle size and density are selected from our previous study and justified below. The study is guided by a number of open questions: Can an oscillator induce a particle towards its own streaming cells, when the particle is initially situated close to another (stationary) cylinder? Such induced motion is not obvious, as the oscillatory flow also sets up a weak streaming flow in the vicinity of the stationary cylinder, with the potential to prevent a particle from escaping. If such induction is possible, is it still so when the particle is shielded from the oscillator by the stationary cylinder? These scenarios arise during transient intervals, after an oscillator's motion has been initiated and the streaming flow is still being established. How does such transience affect the behavior of the particle? If transport from one oscillator to another is possible, are there arrays of oscillators that are more effective in reducing the time of transport?

Before addressing these questions, we first confirm in Section II that our high-fidelity simulations can resolve the flow generated by a single oscillating cylinder by comparing with the analytical solution of this flow field. This validation exercise establishes the appropriate grid spacing and time step size for computations of flows generated by arrays of oscillating cylinders, for which there is generally no analytical solution. Then, in Section III, the streaming flow calculations and transport model are applied in this wider context of multiple oscillators to explore the potential for particle transport in various arrays of oscillating cylindrical probes. We explore the time scales of the particle transport in each array. We also investigate the mechanisms that induce a particle to move toward an oscillator when it originates in the vicinity of another object.

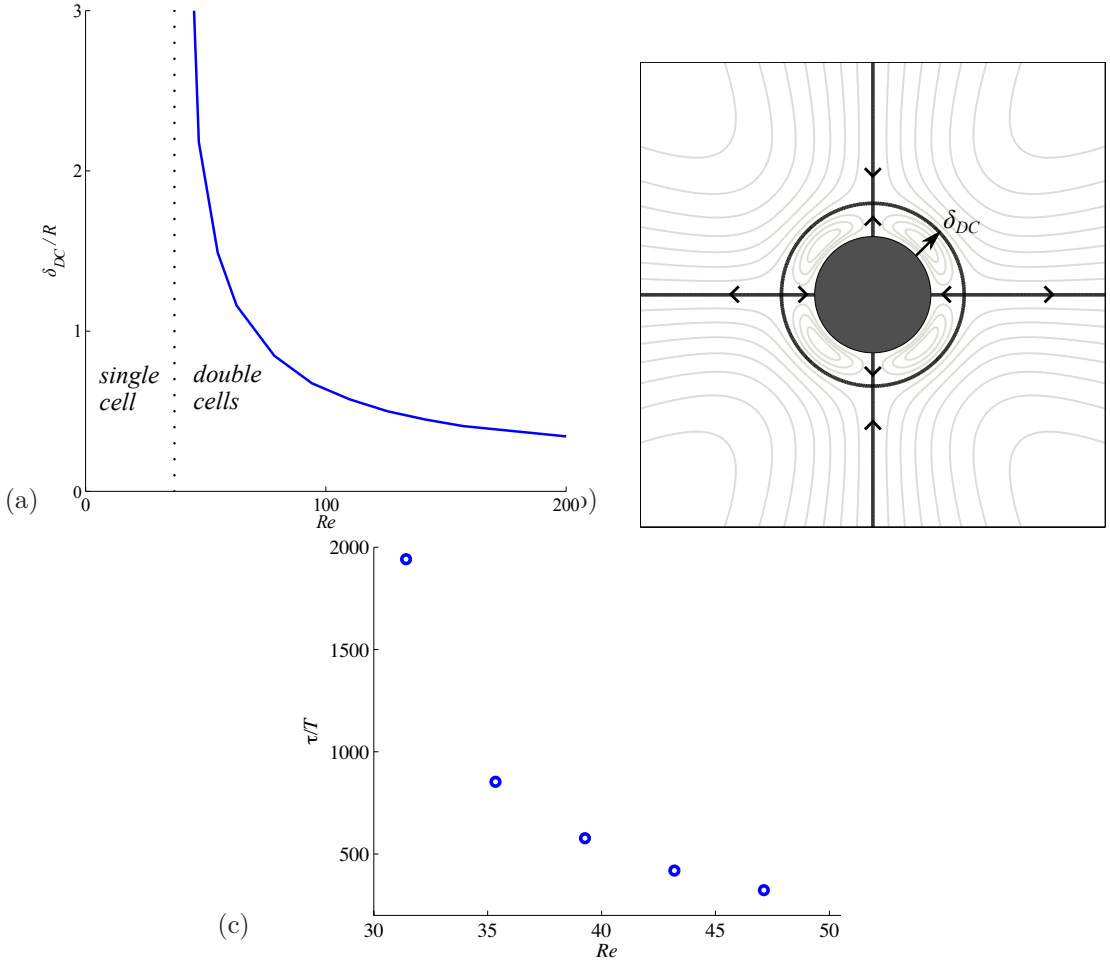

FIG. 2. (a) Inner streaming cell size δ_{DC}/R dependence on Re. (b) The structure of the mean streamlines at $Re = 110$. (c) Trapping timescale dependence on Re for $\rho_p/\rho_f = 1$, with a/R varied so that $\Omega a^2/\nu$ is fixed at 1.2. Reprinted with permission from Chong *et al.*, Phys. Fluids 25, 033602 (2013). Copyright 2013, American Institute of Physics.

II. METHODOLOGY

A. Problem set-up

In the present work, we investigate inertial particle transport in a streaming flow generated by oscillating probes. Probes oscillate in sequence to effect transport of particles between them. Consider an inertial particle whose radius and density are a and ρ_p, respectively, in a streaming flow generated by one or more cylinders with equal radius R. Each cylinder is prescribed with a sinusoidal oscillation along the x-axis, with displacement relative to the mean position described by $A\sin\Omega t$ (as shown for a single cylinder in figure 1(a)) with amplitude A and angular frequency Ω in an otherwise quiescent fluid with kinematic viscosity ν. Each cylinder oscillates for a finite interval in time; the oscillation intervals of each cylinder are sequential and non-overlapping. The Reynolds number for this flow is defined as $Re = \Omega R^2/\nu$ and oscillation amplitude is assumed to be small, $\epsilon = A/R \ll 1$. In our previous work, we showed that it was sufficient to rely on a one-way coupling, wherein the flow field obtained analytically in the absence of particles was used to obtain forces on the particle; the particle's effect on this flow field is ignored since the size of the inertial particle is small compared to the characteristic length of the oscillator, $a/R \ll 1$. Here, we use the same strategy.

It is important to consider the wide range of length and time scales that affect the transport processes in a streaming flow. For example, vorticity is largely confined to a thin Stokes layer $\delta_{AC} \sim Re^{-1/2}R$ and inertial particles are transported inside a streaming cell of size δ_{DC} [12, 17]. As we discuss below, δ_{DC} is of order R or larger in the Reynolds number range of interest for a solitary oscillator, though this size is limited by the presence of other oscillators, so is

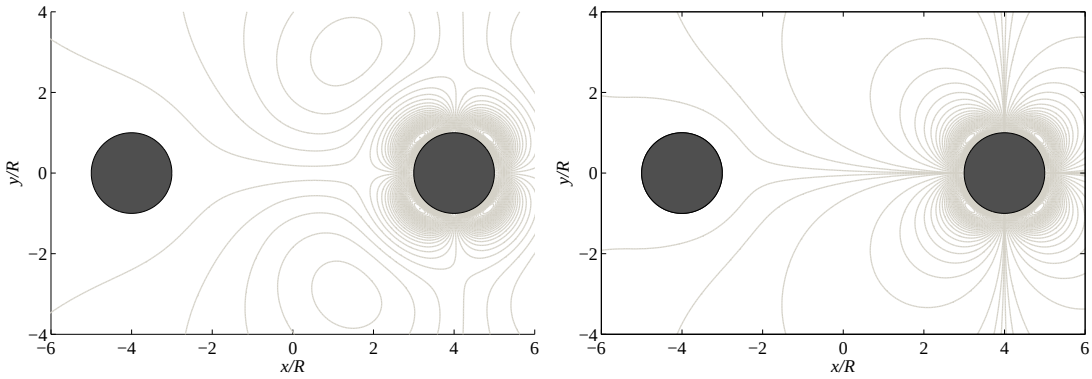

(a) (b)

FIG. 3. Time-averaged Lagrangian streamline generated by high-fidelity numerical simulation (the VVPM) for $Re = 40$, (a) $\epsilon = 0.2$ and (b) $\epsilon = 0.1$

bounded from above by the characteristic distance between oscillators. It therefore takes $O(Re\delta_{DC}^2/R^2)$ oscillations for vorticity to diffuse over this streaming cell, since the time scale to diffuse across a region of size δ_{DC} goes like $\delta_{DC}^2/\nu = Re(\delta_{DC}/R)^2T/2\pi$ (where $T = 2\pi/\Omega$ is the period of oscillation). Inertial particles travel around this cell with characteristic streaming velocity $V_s = \epsilon A\Omega$, so the transport timescale is of order $\delta_{DC}/\epsilon A\Omega = (\delta_{DC}/R)\epsilon^{-2}T/2\pi$. The role of the underlying oscillatory flow in determining the force on the particle cannot be ignored. Due to the importance of the wide range of time and length scales, it is crucial that all scales are sufficiently resolved in the simulation. Thus, our high-fidelity simulations of the flow field resolve the flow down to the oscillatory time scale (50 times steps/period), and the particle trajectories are computed in this full unsteady flow field rather than the time-averaged one.

The Reynolds number controls the size of the streaming cells into which particles are trapped. From previous work, it is known that the streaming flow of an isolated oscillator is composed of an inner streaming cell and an outer streaming cell. As Reynolds number decreases, the inner streaming cell size increases and, when Re approaches 37, the cell becomes boundless, as shown in figure 2(a). Figure 2(b) denotes the inner and outer streaming cells for $Re = 110$. Our previous study [17] demonstrated that an inertial particle initially inside an inner streaming cell remains inside and becomes trapped while a particle outside the cell remains outside. Also, that study found that larger particle size, smaller particle density and higher flow Reynolds number led to faster trapping timescales. (The effect of Reynolds number on trapping time is shown in figure 2(c).) Thus, Reynolds number controls the size of the streaming cell (and thus, the apparent domain from which particles can be trapped) as well as the trapping/transporting speed. A higher Reynolds number flow can effect faster inertial particle transport but the domain of trapping becomes smaller. Though these results do not reflect the transient effects experienced after an oscillator's motion is initiated, which may alter the extent of the trapping domain, they nonetheless provide useful guidance on choosing a set of parameters on which to focus this study.

In an array of oscillators, the behavior is further complicated by the introduction of another length scale, L, the characteristic distance between an oscillator and a nearby obstacle. Thus, whereas ϵ has no effect on the shape and size of streaming cells for an isolated oscillator, it does play a role in an array, since R/L is fixed, so a change to $\epsilon = A/R$ also implies a change to the oscillator's excursions relative to the obstacle, A/L, thereby affecting the streaming cell's behavior. Figure 3(a) depicts the inner and outer streaming cells generated by high-fidelity simulation for $Re = 40$ and $\epsilon = 0.2$. If these conditions are imposed on an isolated cylinder, we expect the inner streaming cell to have characteristic size $\delta_{DC} = 4.6R$. Here, with A/L equal to 0.025, the inner cell's boundary is pushed much closer to the oscillator. By reducing the oscillation amplitude to $\epsilon = 0.1$ and thus reducing A/L to 0.0125, the inner streaming cell is extended outward toward the obstacle, and indeed, the outer streaming cell is apparently annihilated, as shown in figure 3(b). This complex effect of oscillation amplitude on the size of inner streaming cell cannot easily be identified through asymptotic expansion of the Navier–Stokes equations, so it requires high-fidelity simulation. Importantly, for our application here, the domain of trapping can be extended by the presence of nearby obstacles, and this extension is enabled by reducing ϵ (and thus reducing A/L).

Based on this discussion, we focus in this work on streaming flows at a single Reynolds number and oscillation amplitude, $Re = 40$ and $\epsilon = 0.1$, in which the streaming cell is sufficiently large to draw particles from a wide region for trapping and the transporting speed is as fast as possible. However, we should note that the technique is effective over a broader range of Reynolds number. The size and density of the inertial particle are chosen as $a/R = 0.175$ and $\rho_p/\rho_f = 1$, respectively. These choices will not diminish the generality of the qualitative behaviors observed here, but the timescales reported are dependent on the choices. We will address this further in the conclusions of the paper.

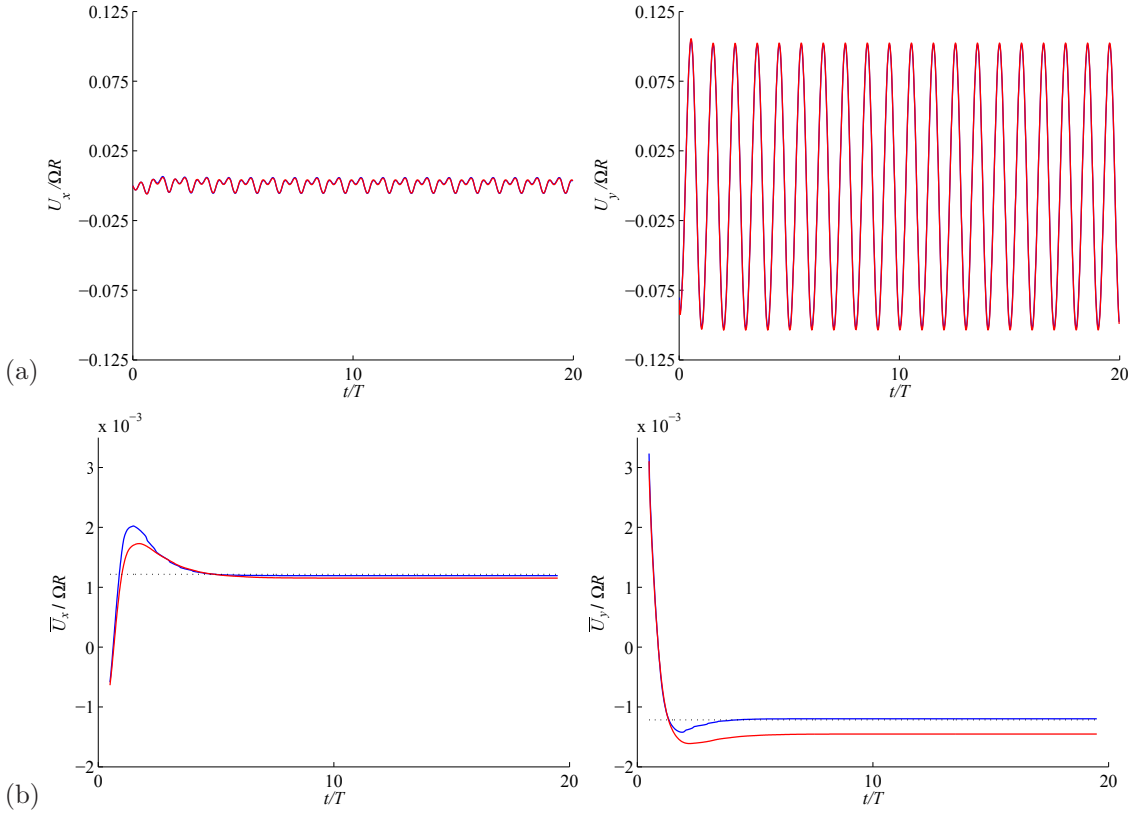

FIG. 4. Time varying velocity history (a) and time averaged velocity history (b) of VVPM for $\epsilon = 0.1$ and $Re = 40$ at $(\sqrt{2}R, \sqrt{2}R)$ during $t/T \in [0, 20]$. Black dotted line denotes the analytical solution. Blue and red solid line indicates the VVPM simulation for $\Delta x = 0.01$ and $\Delta x = 0.02$, respectively.

B. Numerical methodology and validation

Analytical solution for the flow in an array of cylinders is generally not possible, so instead, we rely on high-fidelity numerical computations using the viscous vortex particle method (VVPM) [24], which solves the full Navier-Stokes equations in the vicinity of one or more bodies in arbitrary relative motion. Figure 4 presents both the time-varying and time-averaged velocity generated at a sample point by a single oscillating probe at $Re = 40$, and compares this computed velocity with the analytical solution available for this flow [21]. It shows good agreement between the VVPM and analytical solution and accurately captures the primary as well as the secondary oscillating behavior, the latter apparent in the x component of velocity in figure 4(a), with twice the frequency of the fundamental oscillation. Moreover, the streaming velocity, i.e., the time-averaged (and thus secondary) velocity also exhibits good agreement in figure 4(b). Thus high-fidelity simulations can be used to solve the streaming flow in arrays of cylinders.

It is useful to note that, based on the VVPM simulations, which capture the transient behavior after the cylinder has started from rest, the oscillatory component appears to achieve a stationary form within only one or two oscillation cycles, whereas the time-averaged velocity requires several more oscillations to settle down. This is partly attributable to the fact that the primary oscillatory flow is mainly communicated by pressure, whereas the secondary flow is established more slowly by viscous diffusion.

In this work, we consider transport in various cylinder arrays. The basic strategy can be described with two cylinders, as shown in figure 5. The left cylinder, located at $(-4R, 0)$, is initially oscillated. After an inertial particle is trapped inside the streaming cell of the left cylinder, the oscillation of this cylinder is stopped and the oscillation of the right cylinder located at $(4R, 0)$ is started immediately to instigate the trapped inertial particle to move to the newly established streaming cell of the right cylinder. Figure 5(b) illustrates the oscillation sequences. The flow field is generated by oscillating the left cylinder until $t/T = n_{s1}$ when the streaming flow field has reached a stationary periodic behavior (blue solid line). Then, the flow field from one oscillating cycle after $t/T = n_{s1}$ is repeatedly re-used to numerically integrate the inertial particle trajectory until it is finally trapped at $t/T = n_{f1}$ (blue dotted line). The right cylinder starts to oscillate at $t/T = n_{f1}$ and the flow field is computed until $t/T = n_{s2}$ when the streaming flow reaches stationary periodic behavior again (red solid line). Then, one oscillating cycle after $t/T = n_{s2}$ is again

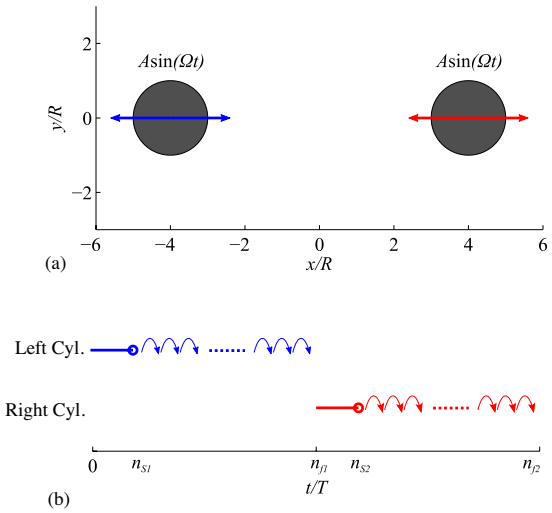

FIG. 5. Schematic of two oscillating cylinders and the sequence of their oscillations. (a) Oscillating two-dimensional cylinders with amplitude A and frequency Ω. (b) Sequence of oscillating cylinders. Velocity field is obtained from high-fidelity simulations during the intervals denoted by horizontal lines, until flow reaches stationary periodic state (open circle). Field from last oscillation cycle in these intervals is repeatedly re-used, indicated by arced arrows, until particles are trapped.

re-used. Meanwhile, the trapped inertial particle is allowed to move freely until it is finally trapped inside the center of the newly established streaming cell at $t/T = n_{f2}$ (red dotted line). In this manner, the high-fidelity solution of the background flow is only required as long as necessary to account for the transient influence from each cylinder's initial motion.

C. Calculation of inertial particle trajectories

As discussed above, attention in this study is restricted to an inertial particle of radius $a/R = 0.175$ and neutral density $\rho_p/\rho_f = 1$, in a flow of Reynolds number $Re = 40$ and amplitude $\epsilon = 0.1$. The motion of an inertial particle inside this flow is calculated from the Maxey-Riley equation [25] with an additional Saffman lift force [23], using the time-varying velocity field predicted by our high-fidelity simulation of the flowfield. Use of this particle transport equation in such a flow is restricted by the condition of small slip Reynolds number, $Re_p = \rho_f a|\boldsymbol{w}|/\mu \ll 1$ (the Reynolds number based on the particle velocity relative to the local undisturbed flow, $\boldsymbol{w}$, and particle radius, a) and small shear Reynolds number, $Re_G = a^2 G/\nu \ll 1$ (the Reynolds number based on the velocity gradient, G), as well as $Re_p \ll Re_G^{1/2}$ [17]. It was verified in our previous work that the simulations of this current flow regime and particle size satisfy these restrictions in every flow field, even inside the Stokes layer, where the inertial particle experiences the largest slip velocity and shear gradient.

The overall transport equation in terms of relative velocity between inertial particle and fluid, $\boldsymbol{w} = \boldsymbol{V}_p - \boldsymbol{u}(\boldsymbol{X}_p)$ and non-dimensionalized by R, Ω and ρ_f, is,

$$\begin{aligned}\left(\frac{\rho_p}{\rho_f}+\frac{1}{2}\right)\frac{\mathrm{d}\boldsymbol{w}}{\mathrm{d}t} = &-\frac{9}{2}Re_a^{-1}\boldsymbol{w}\lambda + (1-\rho_p/\rho_f)\left.\frac{\mathrm{d}\boldsymbol{u}}{\mathrm{d}t}\right|_{\boldsymbol{X}_p(t)} - \frac{3}{2}\boldsymbol{w}\cdot\nabla\boldsymbol{u}\Big|_{\boldsymbol{X}_p(t)} \\ &+ 3KRe_a^{-1/2}|G|^{1/2}\,\mathrm{sgn}(G)|\boldsymbol{w}|\boldsymbol{n} + F\left(\frac{\delta}{\delta_{ss}}\right)e_d W_o \\ &+ \frac{3}{4}Re_a^{-1}(a/R)^2\nabla^2\boldsymbol{u}(\boldsymbol{X}_p(t),t) + \frac{1}{20}(a/R)^2\frac{\mathrm{d}}{\mathrm{d}t}\left[\nabla^2\boldsymbol{u}(\boldsymbol{X}_p(t),t)\right], \end{aligned} \tag{1}$$

where $Re_a = \Omega a^2/\nu = Re(a/R)^2$ is a particle-based Reynolds number. The terms on the right hand side of equation (1) represent, respectively, modified Stokes drag, fluid acceleration force, convective force, Saffman lift, elastic collision force, and Faxén correction terms for the Stokes drag and fluid acceleration force.

Compared to the equation (14) of our previous work [17], in the particle transport equation used here the Basset history force is omitted since its effect was found to be negligible in [17] in the present regime. The transport equation used here also includes two additional modifications that account for the effect of a wall: a lubrication force and an

elastic collision force from direct contact between particle and wall. Both force models are adapted from the work of Li *et al.* [26]. Following [26], the Stokes drag term is modified with a factor λ, in which the lubrication force and Stokes force are blended by $\lambda = 0.5\delta^{-1}H\left(\delta/\delta_{sl}\right)+1-H\left(\delta/\delta_{sl}\right)$, where $H\left(z\right) = \left[1+\exp(10(z-1))\right]^{-1}$ represents a smoothed and shifted Heaviside function, and $\delta = h/(2a)$ denotes the gap distance, h, between wall (surface of cylinder) and particle surface, normalized by particle diameter; δ_{sl} is chosen as 0.5. As the gap distance decreases, lubrication force—manifested by the first term in λ—dominates, whereas the term recovers the Stokes drag force as the gap distance increases. The elastic collision force is modified by the function $F\left(z\right) = \left(\exp(-z)-\exp(-1)\right)/\left(1-\exp(-1)\right)$, where $0 \leq z \leq 1$ and $F\left(z\right) = 0$ for $z > 1$. The critical gap δ_{ss} and the dry coefficient of restitution e_d are set as 0.017 and 0.97, respectively [26]. The details of the force, W_o, which is based on the Hertz elastic force [27], can be found in [26].

It should be stressed that no additional assumptions need be made to use these wall models in the present oscillatory-flow context. Furthermore, these forces are only active, respectively, when the gap distance is $\delta < \delta_{ss}$ and $\delta < \delta_{sl}$, as a particle approaches a cylinder just off the cylinder's oscillation axis. Their role is simply to prevent particles from intersecting the oscillator's perimeter. As we will illustrate in a specific case in the next section, they have negligible role in determining the mechanics of transport and trapping is negligible, since their active intervals are very limited compared to other forces during the transport process. As was shown by Chong *et al.* [17], the trapping process consists of two primary stages: The fluid acceleration force and Faxén correction terms cause the inertial particle velocity to deviate from the fluid velocity. Once the particle develops a non-zero slip velocity, the Saffman lift acts upon it in the presence of a shear flow, and this provides the main mechanism for particle trapping. In contrast, the Stokes drag resists this deviation by driving the relative velocity between inertial particle and fluid to zero.

III. RESULTS

In this section, we describe the particle transport obtained in a variety of different oscillator arrays. In the first scenario, depicted in figure 6, the transport is considered between two cylinders. As shown in figure 6(a), the inertial particle oscillates along its trajectory due to the background oscillatory flow, particularly when closest to the cylinders. For clarity, the trajectories hereafter are sampled once per cycle.

In figure 6(b), the inertial particle starts at $(-2R, 2R)$ and, over the interval $t/T \in [0, 6784]$ (blue line), becomes trapped in the upper right streaming cell generated by the left cylinder. Once the right cylinder starts to oscillate, the trapped inertial particle starts to move toward it, following a streamline near the line of symmetry of the right cylinder's upper left streaming cell. The speed of the particle is relatively low since the streaming motion weakens as the inverse cube of distance from the oscillator [21]. When the particle is close to the right cylinder, both the lubrication force and the collision force become briefly active as the particle migrates upward, as shown in figure 6(c) between two dashed line. These forces become active under similar circumstances in other cylinder arrangements. Finally, the particle is drawn to the center of this new streaming cell and trapped.

It is important to stress that the initial location of the particle when the second cylinder begins to oscillate is actually outside the boundary of the inner streaming cell ($\delta_{DC}/R = 4.6$) generated by an isolated cylinder oscillating at steady state at this Reynolds number. Thus, no trapping would have occurred if this particle were released from this same position under such conditions. For the reasons delineated in Section II, the presence of the other (stationary) cylinder annihilates the boundary of the inner streaming cell. Furthermore, it should be noted that the weak streaming flow established in the vicinity of the left cylinder during the right cylinder's oscillations does not seem to inhibit transport toward the oscillator. This will be discussed in more detail below in the context of another oscillator configuration.

Next, we examine transport of an inertial particle with oscillating cylinders in a triangular arrangement, as depicted in figure 7(a). Each cylinder oscillates parallel to the x axis; the lower left cylinder oscillates first, followed by the lower right, and finally, the upper cylinder. Between the lower left and lower right cylinder, the inertial particle is transported in a similar manner as between two oscillating cylinders in figure 6. The trapped particle in the vicinity of the lower right cylinder starts to migrate toward and is finally trapped by the upper cylinder, following a streamline generated by the motion of that upper cylinder during $t/T \in [105110, 162754]$ (green line). Although it is not shown in this figure, the particle trapped by the upper cylinder is transported back inside the center of the upper right streaming cell of the lower left cylinder during $t/T \in [162755, 239306]$, thereby completing a closed circuit.

Figure 7(b) depicts the distance between the inertial particle ($\boldsymbol{X}_p$) and the trapping point ($\boldsymbol{X}_{trap}$) of each respective oscillator. Each particle transport interval is composed of slow migration (plateau part) and fast trapping (plunging part). This figure indicates that the slowest portion of this circuit occurs between the lower two cylinders. Though these cylinders are slightly farther apart from each other than they are from the upper cylinder, this is not a sufficient explanation for the difference in transport time. Indeed, it is more important that the trapping positions of the lower right and upper cylinders—situated along the line that connects their centers—are significantly closer to each other than the trapping points between the lower two cylinders. Thus, despite the fact that the particle follows a more

arced trajectory between these trapping points, the transport time is significantly shorter.

In figure 8(a), we depict the transport between cylinders arranged in a linear configuration. The cylinders are oscillated in sequence from left to right. As a result, the inertial particle is initially trapped during the interval $t/T \in [0, 6784]$ by the leftmost cylinder (blue line), then migrates toward and is trapped by the center cylinder in $t/T \in [6785, 105109]$ (red line), and is finally trapped by the rightmost cylinder during the interval $t/T \in [105110, 441381]$ (green line). The streaming flow generated by the oscillation of the rightmost cylinder is felt only weakly in the region of the upper left quadrant of the center cylinder. However, even this weak induced motion can draw the particle (albeit slowly) toward the rightmost cylinder following the streamline within the extended region of trapping. Thus, despite the shielding of the particle by the center cylinder, the streaming induces motion in the particle that draws it toward the oscillator. But the transport is much less effective: as indicated by figure 8(b), it takes more than four hundred thousand oscillations to transport the inertial particle approximately from $(-8R, 0)$ to $(8R, 0)$ in a reasonably straight line.

In order to understand the mechanism by which the particle is drawn from behind the stationary center cylinder toward the rightmost oscillator, in figure 9(a) we depict the trajectory of the particle, with arrows indicating the particle slip velocity, $\boldsymbol{w}$, the background fluid velocity, and the total force acting on the particle (that is, the right-hand side of equation (1), quantifying the rate of change of the slip velocity) during the early stages of motion. Note that the sum of the two velocities is necessarily tangent to the inertial particle trajectory. A Lagrangian streamline (a fluid particle trajectory) is depicted in light gray. The direction of the slip velocity component indicates a gradual motion of the particle upward from behind the cylinder. The particle escapes from the obstruction of the cylinder to a region in which the fluid velocity is comparatively stronger. During this period, the rate of change of the slip velocity is weak, but the relative contribution of the slip to the particle's motion decreases, thereby causing the inertial particle's trajectory to merge with the fluid streamline. Figure 9(b) depicts the components of the hydrodynamic forces that affect the slip velocity. The two largest—the Saffman lift force and the Stokes drag—almost exactly balance each other; the other forces— the Faxén correction and convective terms—are also balanced with each other and relatively smaller in magnitude. So overall, there is little net effect on the particle to deviate from the background fluid motion, and the particle then behaves like a fluid particle until it is drawn into the trapping region of the oscillator. This indicates that the weak interaction with the stationary cylinder does not prevent transport toward rightmost cylinder.

As suggested by these results, the overall transport speed can be improved if one can develop trajectories that avoid transport in weak streaming zones created by obstacles and prefer transport between closely-spaced trapping positions. This can be ensured by arranging the oscillating cylinders in a staggered arrangement, as in figure 10(a). This strategy allows a particle to be transported approximately from $(-9R, 0)$ to $(9R, 0)$ with three hundred thousand oscillations. Figure 10(b) indicates that the slow migration intervals have been significantly reduced by the staggered arrangement.

IV. CONCLUSIONS

The transport of an inertial particle in a viscous streaming flow generated by multiple oscillating cylinders has been investigated by integrating particle trajectories in a flow field obtained by high-fidelity numerical simulation. With a controlled sequence of starting and stopping the oscillation of cylinders, an inertial particle is transported from the streaming cell generated by one oscillating cylinder to the next in the sequence, even if the path is obstructed. It has been demonstrated that particles can be predictably transported and trapped in a variety of oscillator configurations. The staggered arrangement minimizes the slow migration intervals.

Overall, we have shown that viscous streaming flows inside various arrangements of oscillating cylinders enable an effective mechanism for particle manipulation. Based on the oscillator arrangements explored in this work, trajectories in a much wider class of oscillator arrays can be predicted. Though this work has focused on demonstrating this transport for only one set of flow conditions and particle parameters, the process would be identical in a wider set of conditions, albeit with different transport times. This study has shown that the streaming cell size, δ_{DC}/R, for the isolated oscillator at steady state can be enlarged in arrays of cylinders, thereby extending the domain from which particles can be trapped. The transient development of the flow and the influence of neighboring stationary cylinders do not prevent the transport and trapping process. However, the effects of Reynolds number, oscillation amplitude and inter-oscillator spacing—particularly in their influence on cell size—remain an important target of study for future work.

It should be noted that, for oscillation frequencies on the order of 100 kHz (at the upper range of frequencies studied by Wang *et al.* [11] for the oscillating bubble actuator) and a probe diameter of 0.5 mm, the transport times in water for the cases studied here are on the order of three seconds. While this does not match the rapid throughput of other particle sorting techniques, the strategy demonstrated here could be useful for more precise manipulation. In our ongoing work, we are investigating the enhanced streaming topology that can be obtained with simultaneous

oscillators to generate faster trajectories. We are also exploring the potential to use this strategy for selective sorting of particles of various sizes and densities.

ACKNOWLEDGMENTS

Support for this work by the National Science Foundation, under Award Nos. CMMI-0969869 and CMMI-1000656, is gratefully acknowledged.

[1] K. Ahn, C. Kerbage, T. P. Hunt, R. M. Westervelt, D. R. Link, and D. A. Weitz, Appl. Phys. Lett. **88**, 024104 (2006).
[2] A. Valero, T. Braschler, N. Demierre, and P. Renaud, Biomicrofluidics **4**, 022807 (2010).
[3] K. Lee, S. Yoon, K. Lee, S. Kim, H. Sung, and S. Kim, Optics Express **20**, 17348 (2012).
[4] M. MacDonald, G. Spalding, and K. Dholakia, Nature **426**, 421 (2003).
[5] P. Y. Chiou, A. T. Ohta, and M. C. Wu, Nature **436**, 370 (2005).
[6] D. Di Carlo, Lab on a Chip **9**, 3038 (2009).
[7] A. J. Chung, D. R. Gossett, and D. Di Carlo, Small **9**, 685 (2013).
[8] M. Tanyeri, E. M. Johnson-Chavarria, and C. M. Schroeder, Appl. Phys. Lett. **96**, 224101 (2010).
[9] P. Marmottant and S. Hilgenfeldt, Proc. Natl. Acad. Sci. **101**, 9523 (2004).
[10] P. Marmottant, J. P. Raven, H. Gardeniers, J. G. Bomer, and S. Hilgenfeldt, J. Fluid Mech. **568**, 109 (2006).
[11] C. Wang, S. V. Jalikop, and S. Hilgenfeldt, Biomicrofluidics **6**, 012801 (2012).
[12] B. R. Lutz, J. Chen, and D. T. Schwartz, Anal. Chem. **78**, 5429 (2006).
[13] B. R. Lutz, J. Chen, and D. T. Schwartz, Phys. Fluids **17**, 023601 (2005).
[14] V. H. L. Tyler A House and D. T. Schwartz, J. Micromech. Microeng. **24**, 045019 (2014).
[15] A. Hashmi, G. Yu, M. Reilly-Collette, G. Heiman, and J. Xu, Lab on a Chip **12**, 4216 (2012).
[16] Y. Xu, A. Hashmi, G. Yu, X. Lu, H. Kwon, X. Chen, and J. Xu, Appl. Phys. Lett. **102**, 023702 (2013).
[17] K. Chong, S. D. Kelly, S. Smith, and J. D. Eldredge, Phys. Fluids **25**, 033602 (2013).
[18] H. Schlichting, Physikal. Z. **33**, 327 (1932).
[19] N. Riley, Mathematika **12**, 161 (1965).
[20] J. Stuart, J. Fluid Mech. **24**, 673 (1966).
[21] J. Holtsmark, I. Johnsen, T. Sikkeland, and S. Skavlem, J. Acoust. Soc. Am. **26**, 26 (1954).
[22] W. P. Raney, J. C. Corelli, and P. J. Westervelt, J. Acoust. Soc. Am. **26**, 1006 (1954).
[23] P. G. Saffman, J. Fluid Mech. **22**, 385 (1965).
[24] J. D. Eldredge, J. Comput. Phys. **221**, 626 (2007).
[25] M. R. Maxey and J. J. Riley, Phys. Fluids **26**, 883 (1983).
[26] X. Li, M. L. Hunt, and T. Colonius, J. Fluid Mech. **691**, 123 (2012).
[27] S. P. Timoshenko and J. N. Goodier, *Theory of Elasticity, 3rd edn.* (McGraw Hill, 1970).

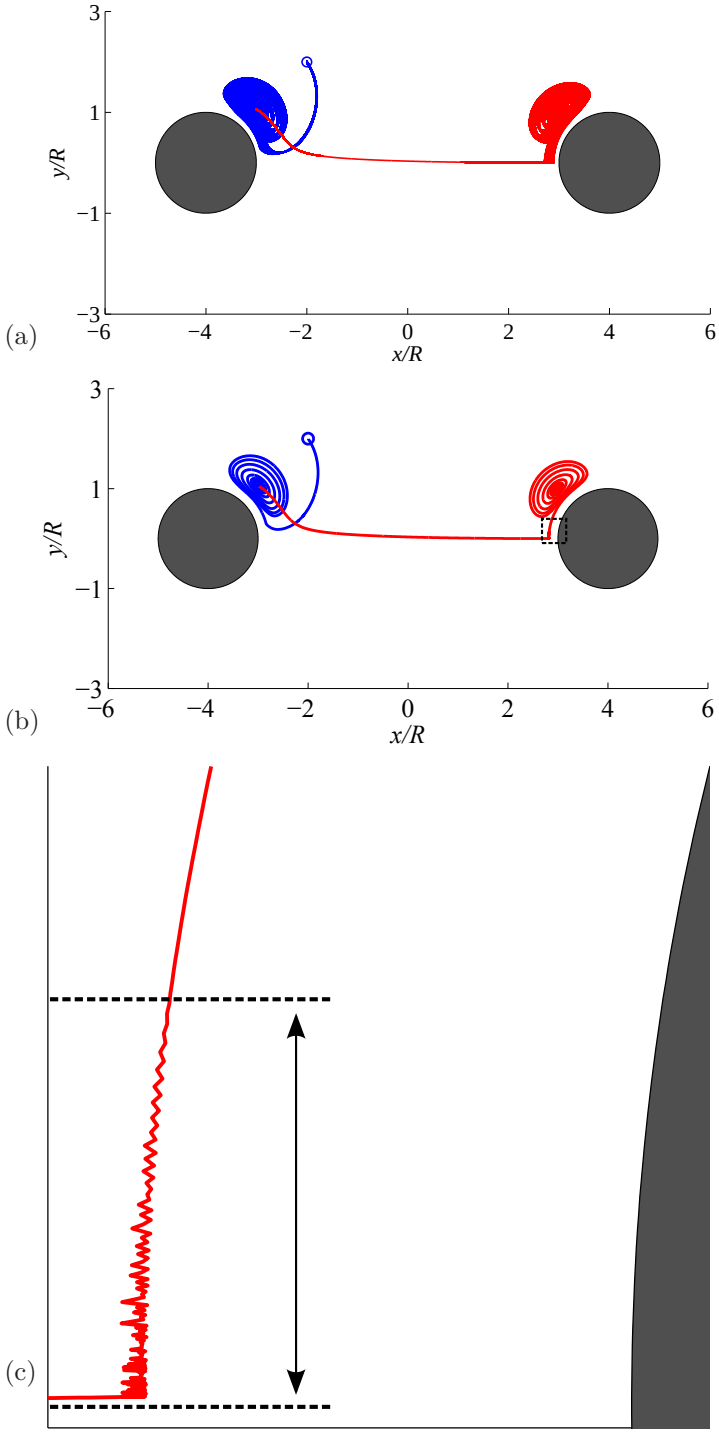

FIG. 6. Inertial particle trajectory between two cylinders. Initial location depicted with blue circle. (a) Continuous inertial particle trajectory, including entire oscillation cycle. (b) Inertial particle trajectory sampled once per cycle. (c) Magnified view of inertial particle trajectory experiencing lubrication and collision forces, corresponding to the dashed box in (b).

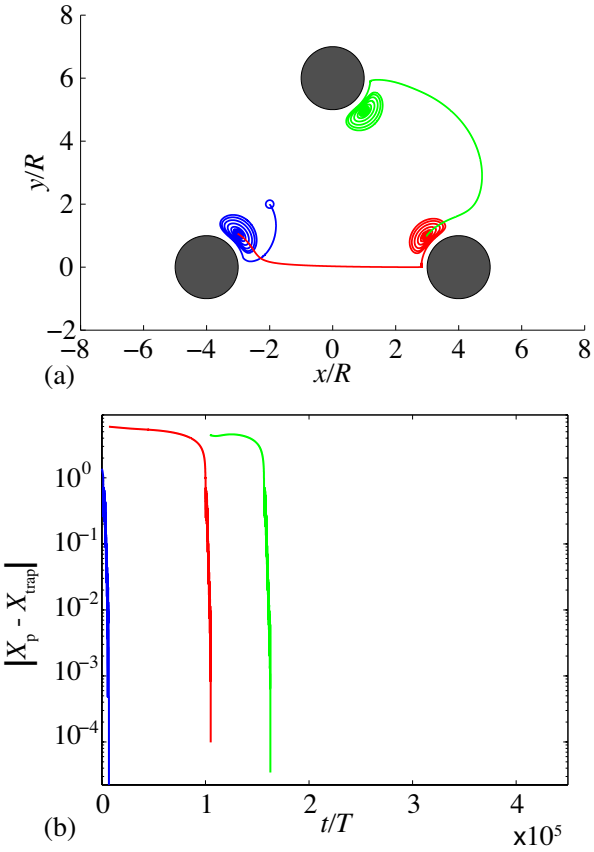

FIG. 7. (a) Inertial particle trajectory in a triangular arrangement. (b) Distance between inertial particle ($\boldsymbol{X}_p$) and trapping points ($\boldsymbol{X}_{trap}$) of each respective oscillator.

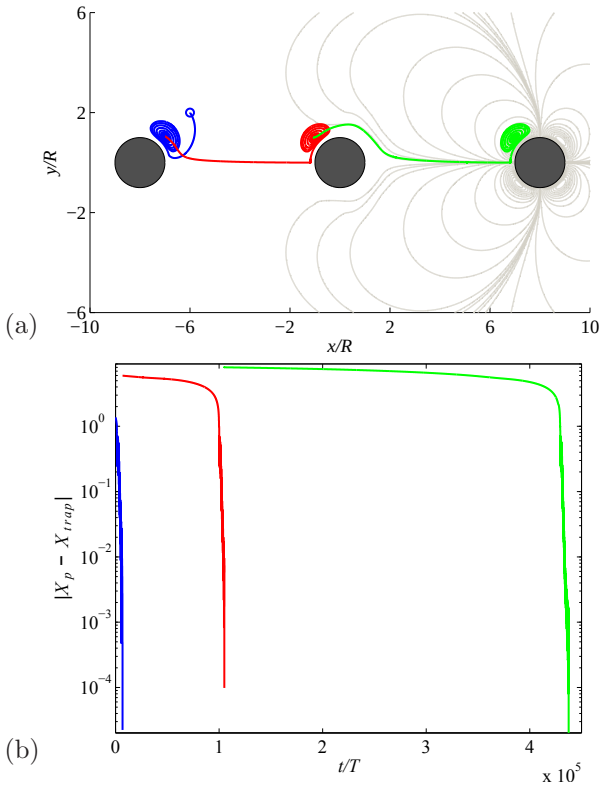

FIG. 8. (a) Inertial particle trajectory in a linear arrangement with time-averaged Lagrangian streamline (gray line). (b) Distance between inertial particle ($\boldsymbol{X}_p$) and trapping points ($\boldsymbol{X}_{trap}$) of each respective oscillator.

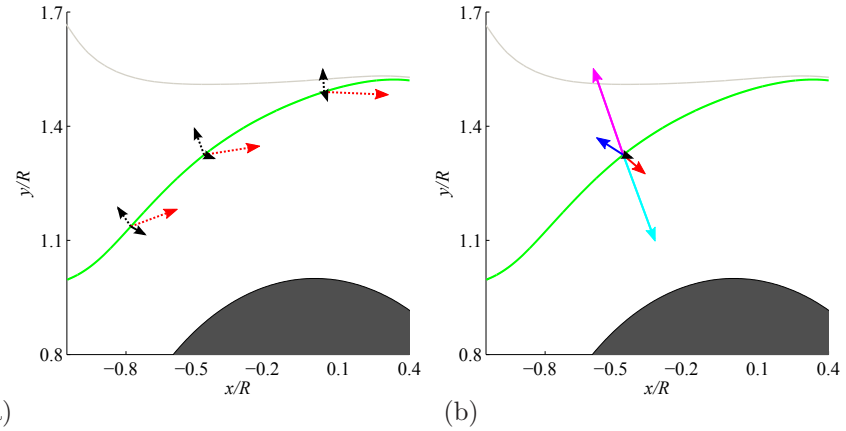

FIG. 9. (a) Hydrodynamic force (black arrow), slip velocity, $\boldsymbol{w}$ (black dotted arrow), and velocity of the background flow (red dotted arrow) experienced by an inertial particle at $(-0.78R, 1.15R)$, $(-0.47R, 1.32R)$, and $(0.04R, 1.50R)$. (b) Component of hydrodynamic forces at $(-0.47R, 1.32R)$: Saffman lift (magenta arrow); Stokes drag (cyan arrow); Faxén correction (blue arrow); convective force (red arrow); net force (black arrow). The Faxén correction, convective force and net force are intentionally magnified to 5 times for visualization purpose.

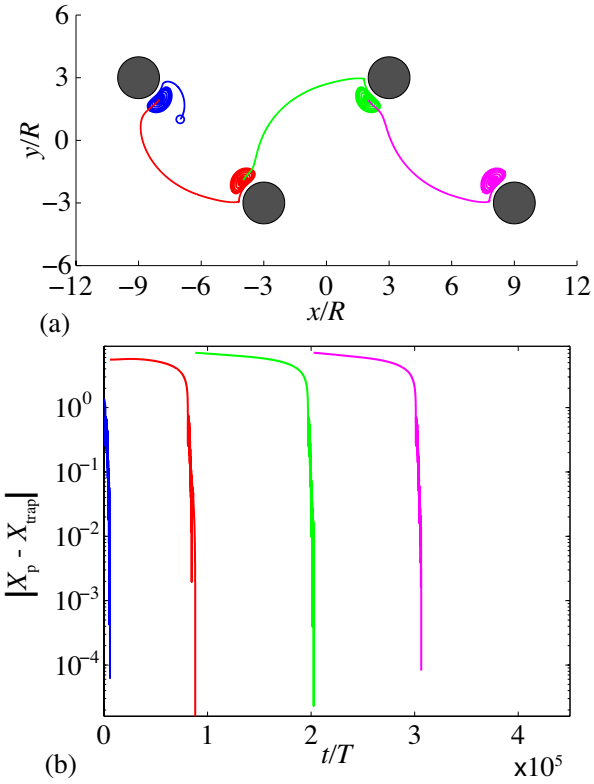

FIG. 10. (a) Inertial particle trajectory in a zigzag arrangement. (b) Distance between inertial particle($\boldsymbol{X}_p$) and trapping points ($\boldsymbol{X}_{trap}$) of each respective oscillator.